

*Special Issue: Artificial Intelligence*

*Scientific Paper*

Doi: <http://dx.doi.org/10.1590/1809-4430-Eng.Agric.v43nepe20210099/2023>

## PREDICTION OF DEM PARAMETERS OF COATED FERTILIZER PARTICLES BASED ON GA-BP NEURAL NETWORK

Xin Du<sup>1,2</sup>, Cailing Liu<sup>1\*</sup>

<sup>1\*</sup>Corresponding author. China Agricultural University/Beijing, China.

E-mail: [cailingliu@163.com](mailto:cailingliu@163.com) | ORCID ID: <https://orcid.org/0000-0001-9190-4117>

### KEYWORDS

coated fertilizer,  
GA-BP neural  
network, angle of  
repose, model fitting,  
triple spline  
interpolation.

### ABSTRACT

To provide an efficient and reliable calibration method with reduced time cost and increased accuracy, the angle of repose (AoR) in the simulation is batch-processed based on Python and the GA-BP neural network is used to improve the prediction accuracy of the DEM parameters of coated fertilizer particles. The single-factor test data were firstly interpolated to obtain sufficient training samples, thus avoiding the drawback that the BP network tends to fall into the local minimum during the training process. Then the GA-BP neural network was trained in combination with the orthogonal combination test, and the fitted correlation coefficients were all greater than 0.975, indicating that the algorithm has strong generalization performance and good stability. The predicted values matched the expected output values, indicating that the GA-BP neural network can accurately predict the nonlinear function output, and the network predicted output can be approximated as the actual output of the function. With the actual AoR as the output value, the simulation value of the AoR was obtained as 24.457° when the coefficient of restitution (CoR), coefficient of static friction (CoSF), and coefficient of rolling friction (CoRF) were 0.509, 0.176, and 0.0332, respectively, and the relative error with the actual value was 0.068%, indicating that the well-fitted GA-BP neural network could accurately predict the DEM parameters of fertilizer particles.

### INTRODUCTION

Particles in a variety of forms – ranging from rock soil to food grains and pharmaceutical powders – play an important role in many industries (Benvenuti et al. 2016; Landry et al., 2006). The Discrete Element Method (DEM) was originally proposed by Cundall & Strack (1979), has been widely used to simulate particle behaviour in these granular processes (Cleary & Sawley, 2002), and can provide a lot of information (such as particle trajectories and interactions) that are difficult to obtain by physical experiments (Chen et al., 2021; Han et al., 2016; Xiao et al., 2021).

To obtain reliable simulation results, the established DEM models should be calibrated first. Researchers have tried many methods to calibrate or measure the discrete

element parameters, and these can generally be divided into two categories: direct calibration and indirect calibration (Beakawi Al-Hashemi & Baghabra Al-Amoudi, 2018; Wang et al., 2020; Zhang et al., 2020). In direct calibration, the particle properties are measured by experiments and directly used as simulation inputs. However, some of the properties are very difficult to measure due to the particle shape and size. In indirect calibration, the macroscopic behaviour of the particles is measured by experiments and then calibrated in reverse by changing a series of simulation parameters until the measured macroscopic behaviour is matched (Xia et al., 2019).

The angle of repose (AoR) is taken as an essential macroscopic parameter in characterizing the flowability of particles. The AoR is defined as the angle between a horizontal surface and the slant height of a conical heap of

<sup>1</sup> China Agricultural University/Beijing, China

<sup>2</sup> Jiangsu Ocean University/Lianyungang, China

Area Editor: Rouverson Pereira da Silva

Received in: 6-28-2021

Accepted in: 12-13-2022



the loose granular material at the critical point when this slope collapses. By comparing the experimental and simulated values of the AoR, the material parameters and contact parameters can be calibrated (Tan et al., 2021). The value of the AoR can be obtained by reading the heap's surface value directly by a protractor and calculating the value with the heap's measured diameter and height. However, there are two non-negligible problems, which are summarized in previous reports (Müller et al., 2021; Tan et al., 2020): lower repeatability (errors between two measurements performed by one operator) and lower reproducibility (errors between the measurements by different operators in different laboratories). Due to the weakness and uncertainty in the calibration of parameters based on the comparison between measured and simulated AoRs, more precise and reliable calibration is necessary for the simulation of irregular materials in DEM industrial applications (Tan et al., 2021).

When calibrating multiple parameters, a large number of experiments are required to ensure the model accuracy, which is time-consuming and inefficient. To make up for the above shortcoming, central composite design (CCD) (Yoon, 2007), the Taguchi method and orthogonal experiments (Hanley et al., 2011), Latin hypercube sampling and the Kriging method (Rackl & Hanley, 2017) are used to generate samples. Then the optimized algorithm consisting of a polynomial response surface (Xia et al., 2019), neural network (Benvenuti et al., 2016), and the radial basis neural network method (Zhou et al., 2018) can be used to process the data and get the calibration results. The above method can reduce the number of experiments, but there is a problem of large relative errors between the measured value and the simulated value due to the large convergence threshold.

Our study aims to provide an efficient and reliable calibration method with reduced time cost and increased accuracy. In order to achieve this goal, the AoR value in the

simulation is batch-processed based on Python to improve the accuracy; the experimental data is iteratively optimized based on the GA-BP neural network to improve the prediction accuracy of the DEM parameters.

## MATERIAL AND METHODS

### DEM modelling of fertilizer granules

In this paper, the film-coated controlled-release compound fertilizers (N-P<sub>2</sub>O<sub>5</sub>-K<sub>2</sub>O 24-6-10) were sourced from Shandong Nongyang Biological Technology Co., Ltd., China (Figure 1b), 100 randomly selected fertilizer granule samples were measured in three directions: length, width, and thickness, using digital calipers (accuracy 0.01 mm), and the average triaxial dimensions of the fertilizer particles were 4.08 mm×3.97 mm×3.89 mm. The equivalent diameter  $D$  and sphericity  $S_p$  were calculated using [eq. (1)] and found to be 3.98 mm and 0.975, respectively, and the size distribution is shown in Figure 1a. A single sphere with an average diameter of 3.98 mm and standard deviation of 0.52 was used in the DEM simulation to build the fertilizer granule simulation model (Figure 1c).

$$\begin{cases} D = \sqrt[3]{LWT} \\ S_p = \frac{D}{L} \end{cases} \quad (1)$$

Where:

$D$  is the equivalent diameter of the fertilizer granules, mm;

$L$  is the length of the fertilizer granules, mm;

$W$  is the width of the fertilizer granules, mm;

$T$  is the thickness of the fertilizer granules, mm,

$S_p$  is the sphericity.

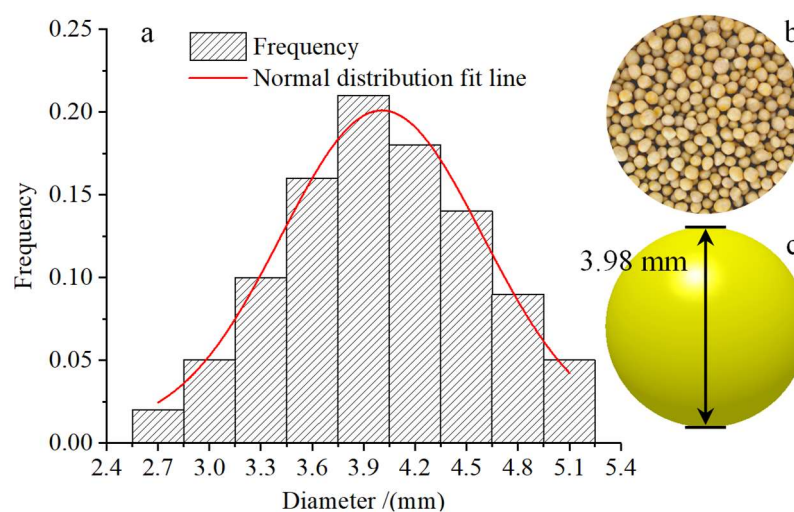


FIGURE 1. Fertilizer particle equivalent diameter distribution (a), actual fertilizer particles (b) and DEM modelling (c).

A random sample of 300 fertilizer granules was selected, and the mass and volume were measured using a digital balance (accuracy 0.001 g) and a measuring cylinder (accuracy 0.01 mL), respectively (drainage method), and the true density of the fertilizer granules was calculated as 1.46 g/cm<sup>3</sup> using [eq. (2)]. The moisture content of the fertilizer granules was measured as 0.88% using a rapid moisture analyzer (accuracy 0.001 g).

$$\rho_{real} = \frac{m_0}{V_1 - V_0} \tag{2}$$

Where:

$\rho_{real}$  is the true density of the fertilizer particles, g/cm<sup>3</sup>;

$m_0$  is the mass of the fertilizer particles, g;

$V_1$  is the total volume of the fertilizer particles and water in the measuring cylinder, cm<sup>3</sup>,

$V_0$  is the volume of water in the measuring cylinder, cm<sup>3</sup>.

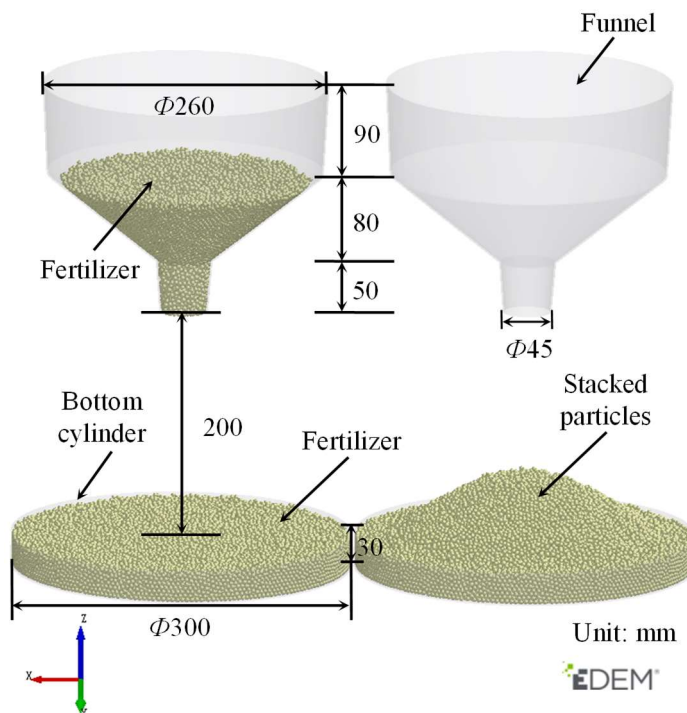


FIGURE 2. AoR simulation test.

In this study, the material which interacts with the fertilizer particles, such as the funnel and the bottom cylinder wheel (Figure 2), is made of ABS (Liu et al., 2018; Zhu et al., 2018). The other discrete element parameters used in this paper are shown in TABLE 1.

TABLE 1. Discrete element parameters.

Parameters	Fertilizer	ABS
Poisson's ratio	0.225(literature)	0.394(literature)
Shear modulus / Pa	1.528×10 <sup>8</sup> (literature)	8.9×10 <sup>8</sup> (literature)
Density / g/cm <sup>3</sup>	1.460(measured)	1.06(literature)
Coefficient of restitution	0.3~0.7(to be calibratd)	0.47(literature)
Coefficient of static friction	0.12~0.24(to be calibratd)	0.42(literature)
Coefficient of rolling friction	0.025~0.045(to be calibratd)	0.095(literature)

**Angle of repose test**

Equipment EDEM2020 of Altair Engineering, Inc. was used to numerically simulate the AoR of the fertilizer particles. Due to the fact that the moisture content of the fertilizer is low, a Hertz–Mindlin (no-slip) contact model was adopted to calculate the particle-particle contact and particle-geometry interactions, as shown in Figure 3. Hertz–Mindlin (No Slip) is

the default model used in EDEM, which is accurate and efficient in force calculation. In this model, the normal force component is based on Hertzian contact theory (Hertz, 1881), and the tangential force model is based on the research work of Mindlin–Deresiewicz (Mindlin, 1949; Mindlin & Deresiewicz, 1953). Both normal force and tangential force have damping components, as described in the literature

(Tsuji et al., 1992) stating that the damping coefficient is related to the restitution coefficient. Tangential friction complies with Coulomb's law of friction; see (Cundall &

Strack, 1979). The rolling friction force is realized by the contact independent directional constant torque model; see (Sakaguchi et al., 1993).

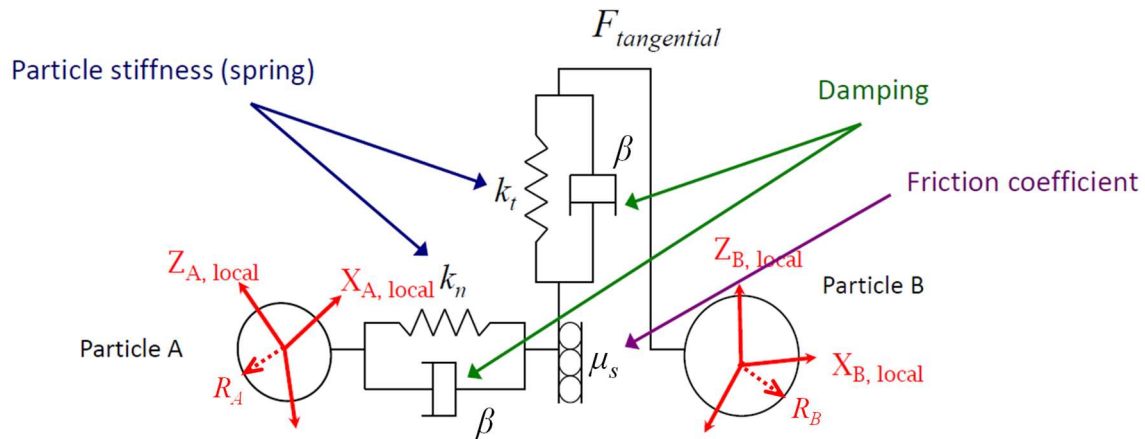


FIGURE 3. Hertz–Mindlin (no-slip) contact model in EDEM.

To accurately reflect the interaction between fertilizer particles, the funnel shown in Figure 2 was used to perform the AoR test on the particles. Firstly, 2500 g and 1000 g of fertilizer particles are generated in the bottom cylinder and funnel, respectively, and the bottom of the funnel is blocked with a plate to prevent particles from falling. After the particles are completely stationary, the simulation file is saved as time 0. Finally, the flat plate at the bottom of the funnel is removed, letting the fertilizer particles fall from a height of 200 mm, and waiting for the particles to be completely discharged and the piled particles to become static. The total simulation time is 4 s, and the time step is  $5 \times 10^{-6}$  s. The data is saved every 0.01 s.

After the simulation has been completed, the AoR

post-processing program based on Python 3.6 is run to connect the EDEMpy library, and the calculation theory is as shown in Figure 4. Firstly, the particle pile is evenly divided into  $n$  parts every  $\theta$  degree, and  $n$  particle slices are obtained; secondly, each slice is divided into two parts, low domain and high domain, then the low domain is divided into multiple bins, the surface particles in each bin are found and their position information is read; lastly, the AoR can be obtained by linear fitting of the surface particles in multiple bins, and the AoR of multiple slices is counted to obtain the mean value and standard deviation. In this research, 18 sampling surfaces were set up on the fertilizer particle pile surface, the bin diameter was 10 mm, and the calculation process is as shown in Figure 5.

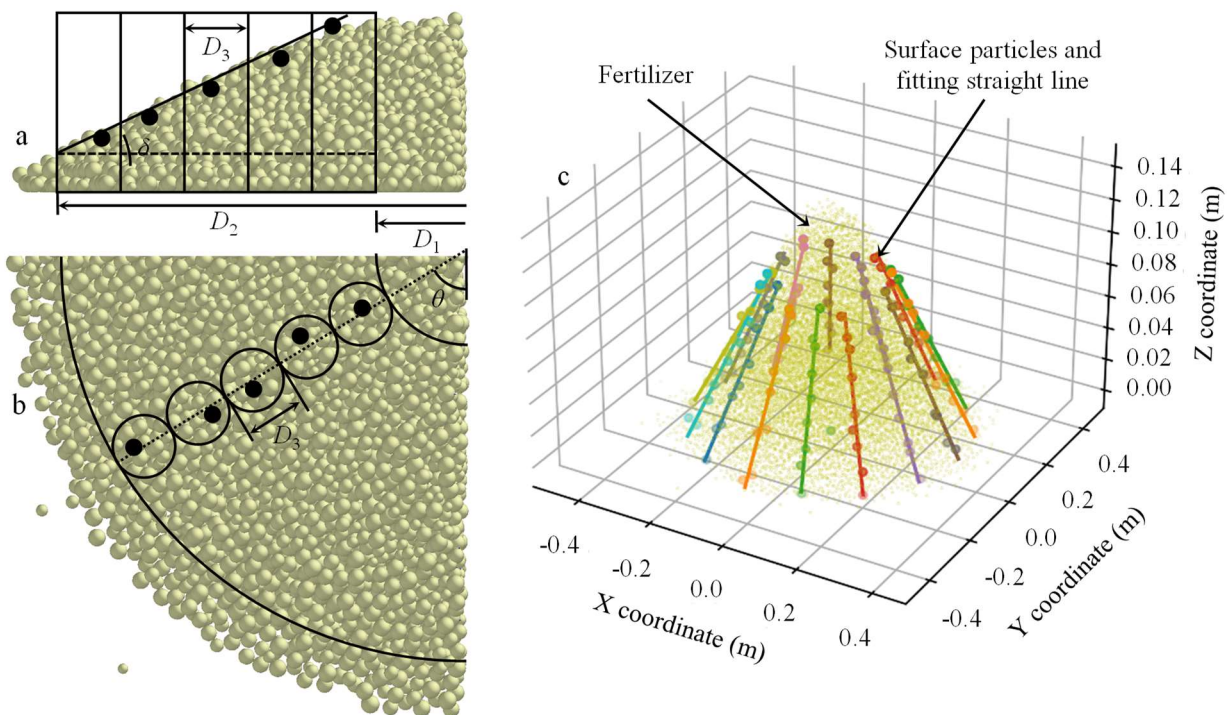


FIGURE 4. Determination of the AoR test using a lifting cylinder (a. front view, b. top view) and measurement on the simulated granular pile (c).

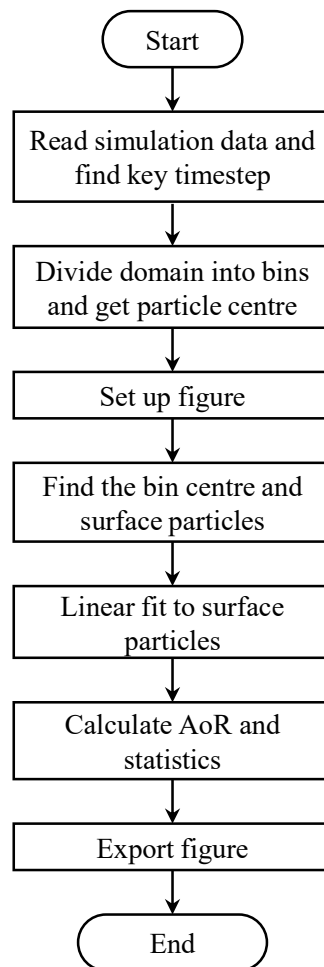


FIGURE 5. Calculation process of AoR.

### GA-BP neural network optimization method

The Back Propagation (BP) neural network algorithm is a kind of neural network of a feedforward learning algorithm and back propagation algorithm, which can effectively solve the problem of the connection weight of the hidden layer in multi-layer neural networks and improve the self-learning and organization ability of the neural network. The Genetic Algorithm (GA) is a random and parallel search optimization method that simulates the natural genetic mechanism and biological evolution theory. This method introduces the biological evolution theory of “survival of the fittest” and has the advantages of high efficiency, parallel, and global search. The GA-BP integrated optimization

algorithm has two main steps, training and simulation of the BP neural network and extreme value optimization of the genetic algorithm. Training and fitting of the neural network mainly includes establishing the BP neural network, which is trained by inputting and outputting data with a nonlinear function, and prediction of the function output. The extreme value optimization process of the genetic algorithm is mainly the prediction result of the neural network as the individual fitness value, and the global optimal value and the corresponding input value are found through selection operation, cross-operation and mutation operation (Qi et al., 2019). The flowchart of the algorithm based on Matlab2016a is shown in Figure 6.

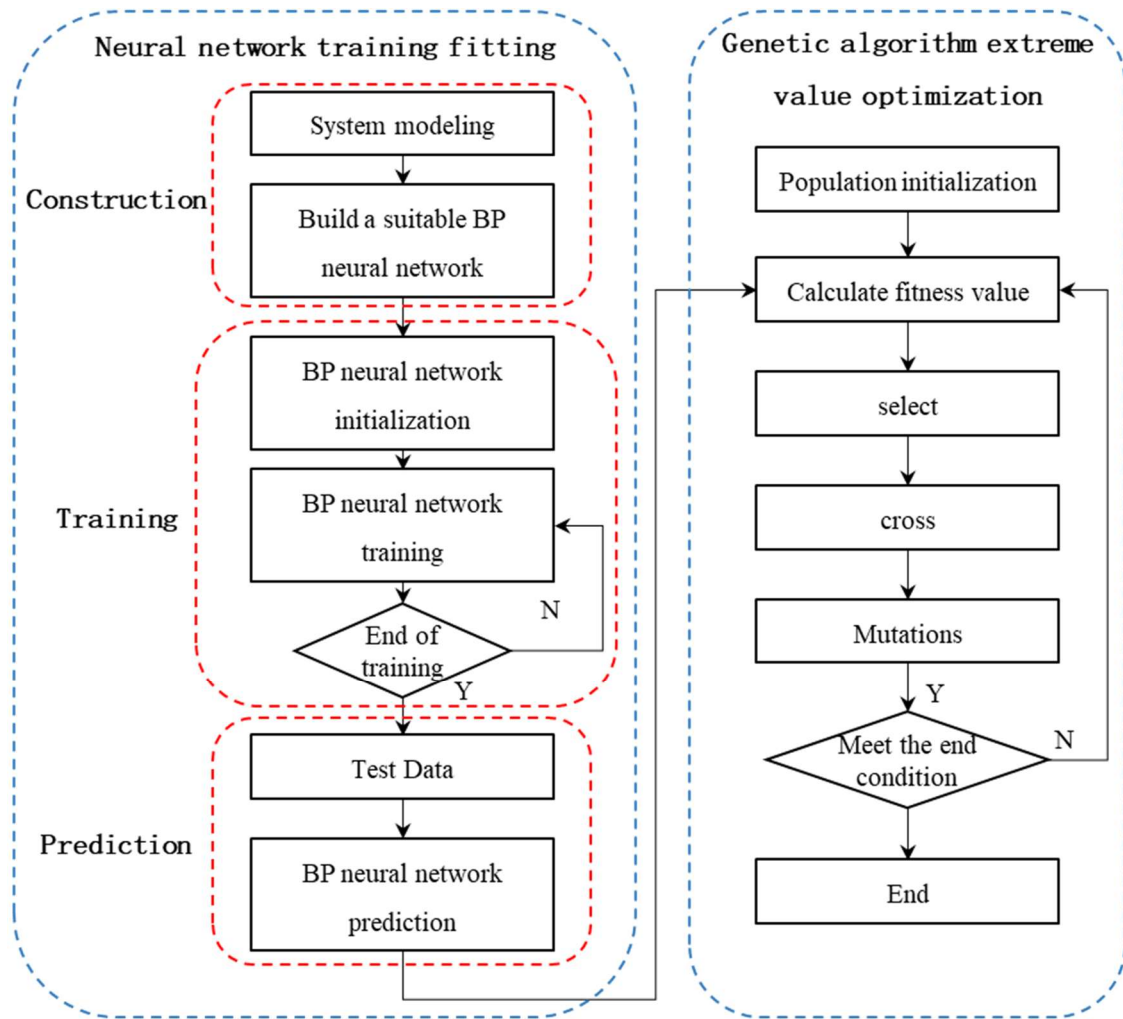


FIGURE 6. Algorithm flow.

In this paper, a 3-layer BP neural network (input layer, hidden layer, and output layer) was used to create an optimization model of the inter-particle contact parameters and AoR, and a total of 3 variables were selected: inter-particle CoR  $x_1$ , CoSF  $x_2$ , and CoRF  $x_3$ , i.e., the number of neurons in the input layer is 3, and the number of objective function AoR  $y_1$  is 1, i.e., the number of neurons in the output layer is 1. The number of neurons  $j$  in the hidden layer is calculated (Equation 3).

$$j = \sqrt{i + k} + z \quad (3)$$

Where:

$j$  is the number of neurons in the hidden layer;

$i$  is the number of neurons in the input layer;

$k$  is the number of neurons in the output layer, and

$z$  is the empirical value ( $1 \leq z \leq 10$ ).

The number of neurons in the hidden layer was calculated to be 3~13, and the best number of neurons in the hidden layer was finally determined to be 10 by the analysis and comparison of the results of previous program running. The structure of the BP neural network is shown in Figure 7.

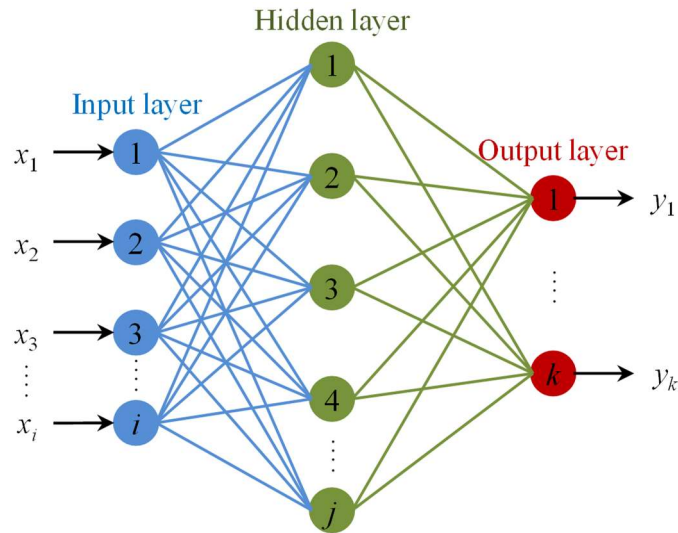


FIGURE 7. BP neural network structure.

The transfer functions of the hidden layer and output layer were a tansig function and Purelin function, respectively, and the objective function between the AoR and the inter-particle contact parameters can be expressed as

$$Y = F(X) = f[V \cdot f(W \cdot X + \theta_1) + \theta_2] \quad (4)$$

Where:

$f()$  is the single-level Sigmoid function of the transfer function from the input layer to the hidden layer and from the hidden layer to the output layer of the BP neural network;

$X$  is the input vector,  $X = [x_1, x_2, x_3, x_4]^T$ ;

$Y$  is the output vector,  $Y = [y_1]$ ;

$F(X)$  is the relationship between the input and the output;

$W$  is the weight matrix of the input layer and the hidden layer;

$\theta_1$  is the threshold of the hidden layer;

$V$  is the weight matrix of the hidden layer and the output layer,

$\theta_2$  is the threshold of the output layer.

To eliminate the quantitative relationship between the input and output vectors, satisfy the value domain interval of the transfer function, and set the input signal too large to cause network output saturation, the training samples are normalized. Let the normalization process interval be  $[a, b]$ , then the input and output data normalization process is calculated as

$$T'_i = a + (b - a) \cdot \frac{T_i - T_{i\min}}{T_{i\max} - T_{i\min}} \quad (5)$$

Where:

$T_i$  is the No.  $i$  input of the training sample data;

$T'_i$  is the normalized data of  $T_i$ ,  $T'_i \in [a, b]$ ;

$T_{i\max}$  is the maximum value of the No.  $i$  input in the training sample,

$T_{i\min}$  is the minimum value of the No.  $i$  input in the training sample.

The inverse normalization formula of [eq. (5)] is

$$T_i = T_{i\min} + (T'_i - a) \cdot \frac{T_{i\max} - T_{i\min}}{b - a} \quad (6)$$

In this paper, the normalization interval  $[0.1, 0.9]$  is selected, and the BP neural network model with the inter-particle contact parameters and AoR adopts a 3-10-1 network structure with an initial learning rate of 0.8, and the mean square error between the actual and desired outputs of the network is less than  $1 \times 10^{-7}$  when the weight matrix and threshold values of the input and hidden layers are saved.

The predicted output of the trained BP neural network was taken as the individual fitness value for genetic algorithm optimization calculation, and the optimal values and corresponding input values of the function were found through selection, interlace operation, and mutation operations. The genetic algorithm parameters were set as follows: the population size, the number of evolutions, the crossover probability and the variation probability are 20, 50, 0.4 and 0.2, respectively, the floating point number is encoded, and the individual length is 3. The individual parameters mainly include the individual fitness function trained by the BP neural network, the population size evolution algebra, the variable function, the optimal fitness value, and the optimal individual of each generation of the population.

## RESULTS AND DISCUSSION

### Coefficient of restitution

The relationship between the CoR and the AoR of the fertilizer particles is shown in Figure 8, when the coefficient of static friction (CoSF) and coefficient of rolling friction (CoRF) are 0.18 and 0.035, respectively, and the CoR is 0.3~0.7.

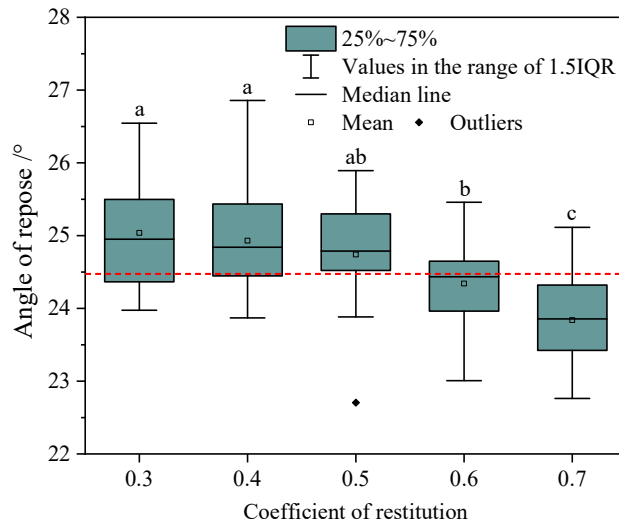


FIGURE 8. Effect of coefficient of restitution factor on AoR.

One-way Analysis of Variance (ANOVA) showed that the homogeneity of the variance test result was significant at  $0.694 > 0.05$ , and the ANOVA result (TABLE 2) showed  $P < 0.0001$ , indicating that there was a significant difference in the effect of the CoR on the AoR. The AoR

decreased with the increase of CoR, and the bigger the CoR, the more quickly the AoR decreased and the more significant the difference between groups. When the CoR is 0.5 and 0.6, the AoR is closer to the actual value (red line), and the degree of fluctuation is correspondingly smaller.

TABLE 2. The ANOVA table.

		Sum of squares	df	Mean square	F	Sig.
CoR	Between-group	17.361	4	4.340	9.175	<0.0001
	Within-group	40.209	85	0.473		
	Total	57.570	89			
		Sum of squares	df	Mean square	F	Sig.
CoSF	Between-group	396.570	4	99.142	252.281	<0.0001
	Within-group	33.404	85	0.393		
	Total	429.974	89			
		Sum of squares	df	Mean square	F	Sig.
CoRF	Between-group	101.818	4	25.455	48.907	<0.0001
	Within-group	44.240	85	0.520		
	Total	146.059	89			

**Coefficient of static friction**

The relationship between the CoSF and the AoR of the fertilizer particles is shown in Figure 9, when the CoR and CoRF are 0.5 and 0.035, respectively, and the CoSF is 0.12~0.24.

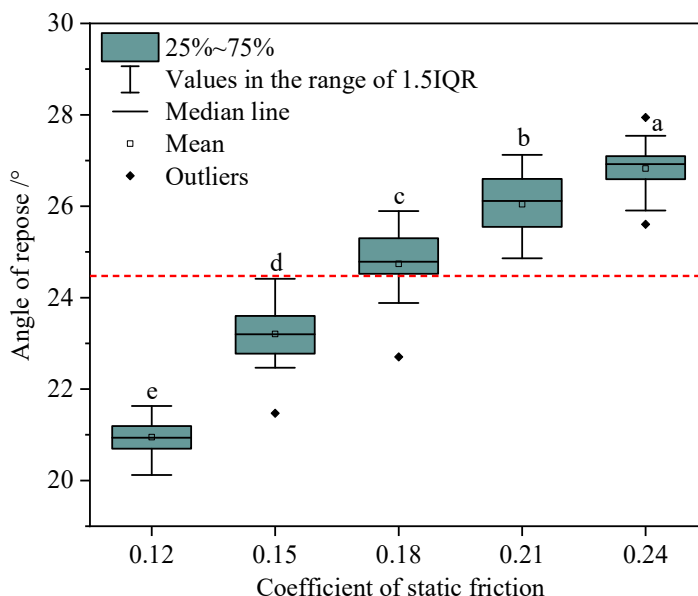


FIGURE 9. Effect of static friction coefficient on AoR.

One-way ANOVA showed that the homogeneity of the variance test result was significant at  $0.265 > 0.05$ , and the ANOVA result (TABLE 2) showed  $P < 0.0001$ , indicating that there was a significant difference in the effect of the CoSF on the AoR. The AoR increases with the increase of the CoSF, and the larger the CoSF, the smaller the degree of increase of the AoR. When the CoSF is 0.15 and 0.18, the AoR is closer to the actual value (red line), and the degree of

fluctuation is correspondingly smaller.

#### Coefficient of rolling friction

The relationship between the CoRF and the AoR of the fertilizer particles is shown in Figure 10, when the CoR and CoSF are 0.5 and 0.18, respectively, and the CoRF is 0.025~0.045.

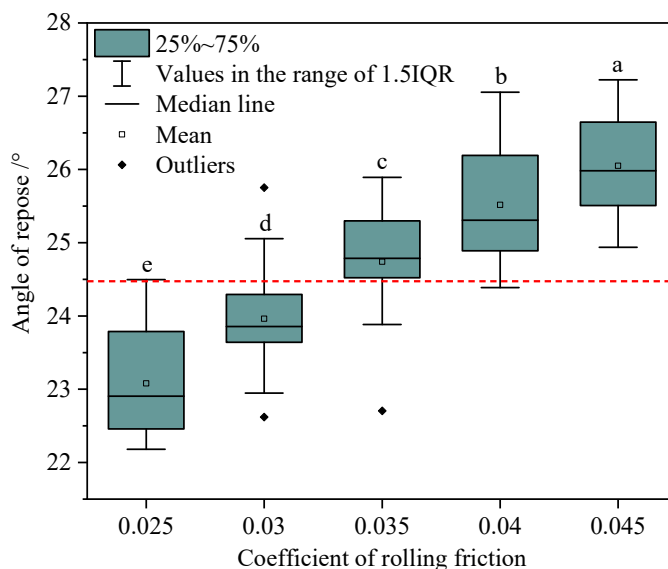


FIGURE 10. Effect of coefficient of rolling friction on AoR.

The one-way ANOVA showed that the homogeneity of the variance test result was significant at  $0.875 > 0.05$  and the ANOVA result (TABLE 2) showed  $P < 0.0001$ , indicating that there was a significant difference in the effect of the CoRF on the AoR. The AoR increased with the increase of the CoRF between the particles, and the larger the CoRF, the smaller the increase of the AoR. When the CoRF is 0.30~0.35, the AoR is closer to the actual value (red line), and the degree of fluctuation is the least.

#### Triple spline interpolation

The single-factor test samples obtained in the above can reflect the effect of the fertilizer particle contact parameters on the AoR, but the number of samples is not sufficient for training the GA-BP network. To solve this problem, an interpolation method is used in this paper. Interpolation is a mathematical method with the following mathematical definition (Bramble & Hilbert, 1970; Mackay, 1992):

The function  $y=f(x)$  has different values  $(y_0, y_1, \dots, y_n)$  at different points  $(x_0, x_1, \dots, x_n)$  obtained by an experimental or measured method. Then, a function  $\Phi(x)$  is constructed for an approximate expression of  $y=f(x)$ , i.e.:

$$y=f(x) \approx \phi(x) \tag{7}$$

Where:

$\Phi(x_0)= y_0, \Phi(x_1)= y_1, \dots, \Phi(x_n)= y_n$ .  $y=f(x)$  represents the interpolated function.

$\Phi(x)$  represents the interpolation function, and  $x_0, x_1, \dots, x_n$  represent interpolation points.

Spline interpolation establishes a cubic polynomial function between adjacent data points to determine the function value of the interpolated data points. The interpolation curve and derivative of spline interpolation are continuous, which results in better smoothness. Therefore, for a better interpolation effect, the spline interpolation method was chosen to interpolate the original data in this paper (Dong et al., 2020).

The CoR, CoSF and CoRF were segmented by triple spline interpolation (Figure 11), and seven interpolation points were selected between two adjacent original points on the interpolation curve; 33 sets of data could be obtained after interpolation analysis, and a total of 99 sets of data were obtained for the three factors.

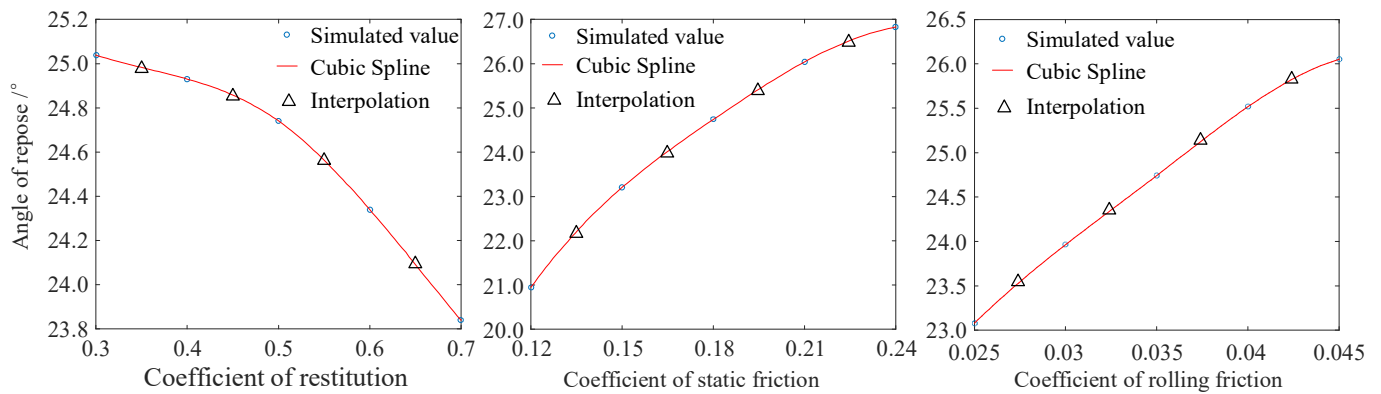


FIGURE 11. Segmented cubic spline interpolation curve.

The results show that the relative errors between the interpolated data and the simulated original values are 0.193%~1.035%, which are very small, and the interpolated data can be considered as the simulated values.

**GA-BP neural network optimization**

Since the effect of interaction between factors was not considered in the previous paper, a CCD experiment was designed to refine the network information, and the experimental design and results are shown in TABLE 3.

TABLE 3. CCD test program and results.

No.	CoR	CoSF	CoRF	AoR / °
1	0.40	0.15	0.0300	22.8850
2	0.70	0.15	0.0300	21.9785
3	0.40	0.21	0.0300	25.2489
4	0.70	0.21	0.0300	23.8707
5	0.40	0.15	0.0400	23.5763
6	0.70	0.15	0.0400	23.4178
7	0.40	0.21	0.0400	27.0148
8	0.70	0.21	0.0400	25.6742
9	0.30	0.18	0.0350	24.8131
10	0.80	0.18	0.0350	22.9109
11	0.55	0.13	0.0350	21.7858
12	0.55	0.23	0.0350	26.5836
13	0.55	0.18	0.0266	23.1235
14	0.55	0.18	0.0434	25.6804
15	0.55	0.18	0.0350	24.6826

Combining the data obtained by the three times segmented spline interpolation, there is a total of  $99+15=114$  sets of data, of which 80 sets of data are selected as the training network and 34 as the validation and testing data. To eliminate the chance factor and obtain a better prediction model, the GA-BP network was trained 20 times, and the correlation coefficients of the training process, validation process, testing process, and overall performance were obtained as shown in Figure 12, respectively.

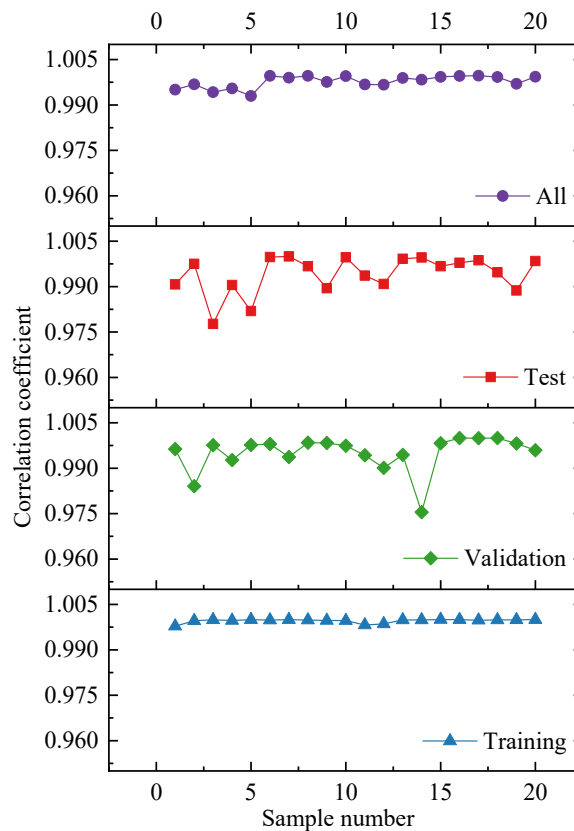


FIGURE 12. Correlation coefficient of the prediction model.

From Figure 12, it can be seen that the correlation coefficients of the training process, validation process, testing process and overall performance are all greater than 0.975. Usually, when the correlation coefficient is greater than 0.9, the fitting performance of the network is considered acceptable, indicating that the GA-BP neural network optimization algorithm has better generalization performance and stability.

As shown in Figure 13, the correlation coefficients of the training process, validation process, testing process and overall performance of the GA-BP neural network are approximately 0.99980, 0.99992, 0.99871 and 0.99967, respectively.

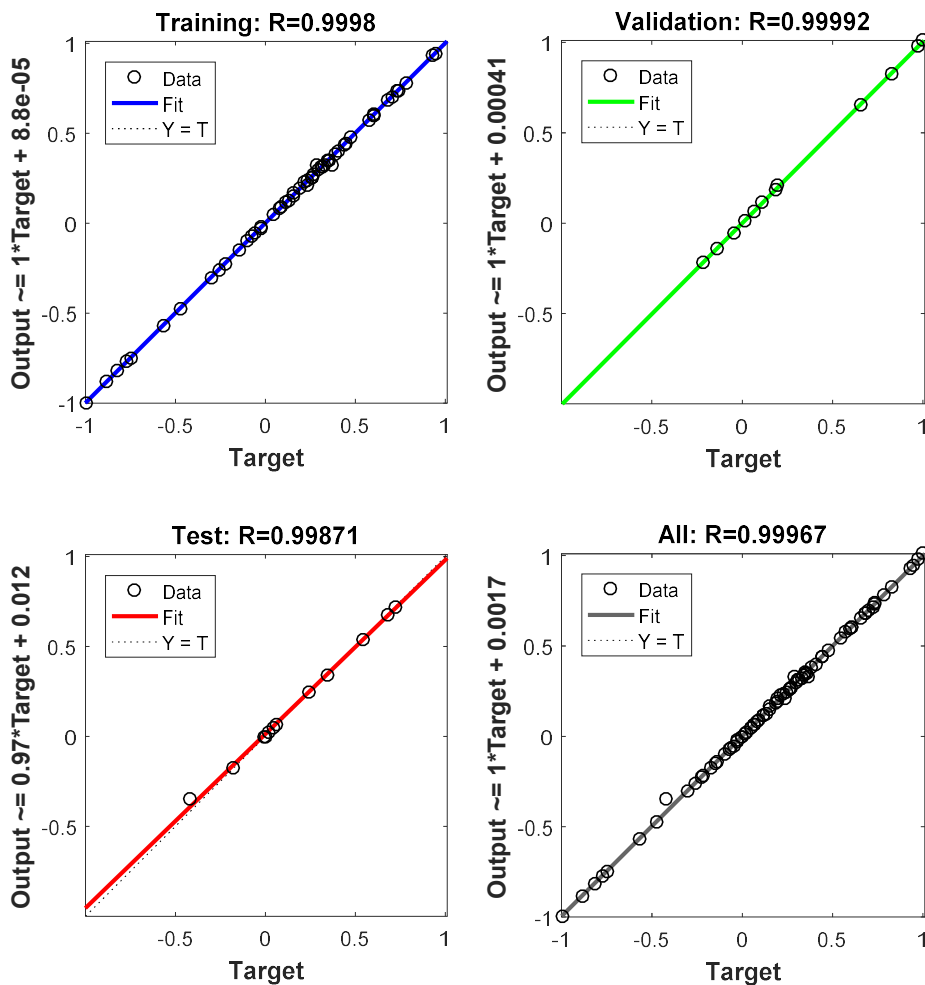


FIGURE 13. Correlation coefficients of GA-BP neural network.

A comparison of the predicted and expected values of the GA-BP neural network model training is shown in Figure 14. As the figure shows, the predicted output values and the expected values match, indicating that the GA-BP neural network can accurately predict the nonlinear function output, and the network predicted output can be approximated as the actual output of the function.

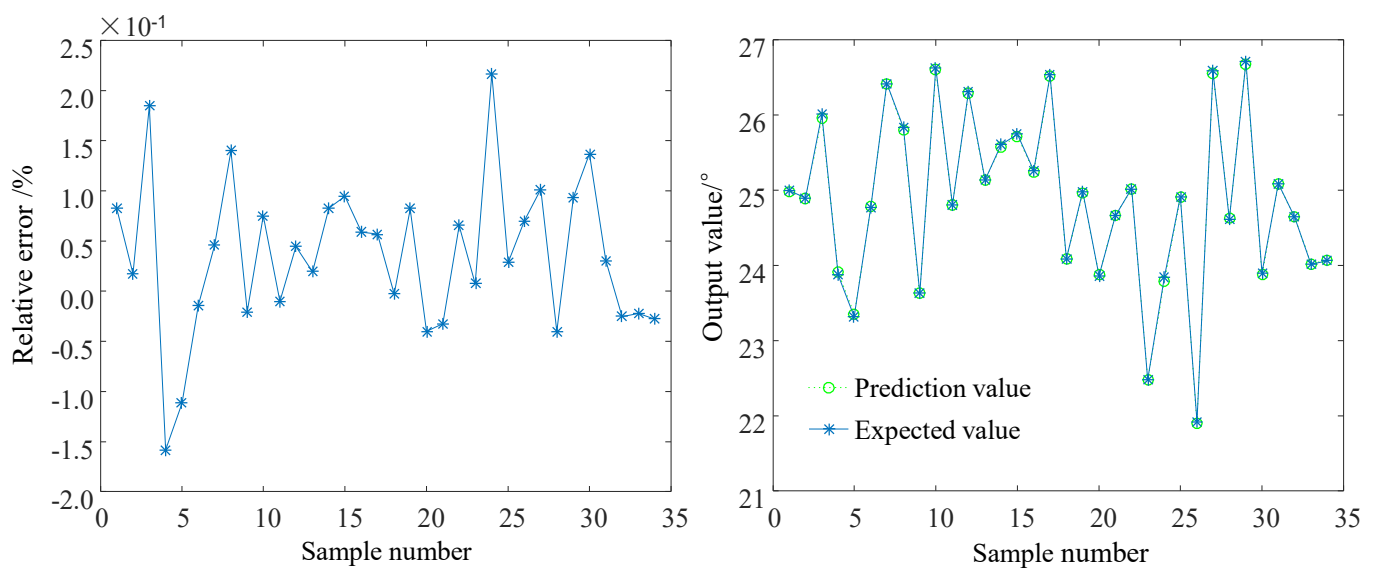


FIGURE 14. BP neural network model fitted values versus experimental values.

With the above trained BP neural network model as the objective function, the inter-particle contact parameters and the AoR were optimized using the optimization method proposed in this paper, and a series of parameter combinations were obtained by solving the network input so that the network output was 24.474° (the actual stacking angle), and the parameters were inverted to verify the rationality of the parameter combinations in EDEM (as shown in TABLE 4).

TABLE 4. Parameter combination verification results.

No.	CoR	CoSF	CoRF	Predicted value /°	Simulation value /°	Relative error /%
1	0.502	0.175	0.0336		24.128	1.415
2	0.511	0.175	0.0332		24.155	1.303
3	0.504	0.176	0.0339	24.474	24.346	0.524
4	0.509	0.176	0.0332		24.457	0.068
5	0.502	0.177	0.0336		24.604	0.532

As can be seen from TABLE 4, the relative errors between the simulated and predicted values of the AoR (i.e., the actual value of the AoR) under various parameter combinations are different, but they are all less than 1.5%, indicating that the GA-BP neural network model obtained from the training is highly accurate. When the CoR, CoSF and CoRF are 0.509, 0.176 and 0.0332, respectively, the simulation value of the AoR is obtained as 24.457°, and the relative error with the actual value is very small, only 0.068%, and this parameter combination can be used as the DEM simulation parameters of the coated fertilizer particles.

## CONCLUSIONS

The AoR value in the simulation is batch-processed based on Python to improve the accuracy.

Sufficient training samples are obtained by data interpolation to avoid the drawback that BP networks tend to fall into the minimum value point during training. The correlation coefficients fitted by the GA-BP neural network after 20 training sessions were all greater than 0.975, indicating that the algorithm has strong generalization performance and good stability.

The predicted and expected output values match, indicating that the GA-BP neural network can accurately predict the nonlinear function output, and the network predicted output can be approximated as the actual output of the function.

Taking the actual AoR as the output value, the simulation value of the stacking angle is 24.457° when the CoR, CoSF and CoRF are 0.509, 0.176 and 0.0332, respectively, and the relative error with the actual value is 0.068%.

## ACKNOWLEDGMENTS

This work was financially supported by National Key Research and Development Plan of China (2017YFD0700703-03).

## REFERENCES

Beakawi Al-Hashemi HM, Baghabra Al-Amoudi OS (2018) A review on the angle of repose of granular materials. *Powder Technology* 330: 397-417. DOI: <http://doi.org/10.1016/j.powtec.2018.02.003>.

Benvenuti L, Kloss C, Pirker S (2016) Identification of DEM simulation parameters by Artificial Neural Networks and bulk experiments. *Powder Technology* 291: 456-465. DOI: <http://doi.org/10.1016/j.powtec.2016.01.003>.

Bramble JH, Hilbert SR (1970) Estimation of linear functionals on Sobolev space with application to Fourier transforms and spline interpolation. *Siam Journal On Numerical Analysis* 7(1):112. DOI: <http://doi.org/10.1137/0707006>.

Chen P, Han Y, Jia F, Meng X, Xiao Y, Bai S (2021) DEM simulations and experiments investigating the influence of feeding plate angle in a rubber-roll paddy grain huller. *Biosystems Engineering* 201: 23-41. DOI: <http://doi.org/10.1016/j.biosystemseng.2020.11.003>.

Cleary PW, Sawley ML (2002) DEM modelling of industrial granular flows: 3D case studies and the effect of particle shape on hopper discharge. *Applied Mathematical Modelling* 26(2): 89-111. DOI: [http://doi.org/10.1016/S0307-904X\(01\)00050-6](http://doi.org/10.1016/S0307-904X(01)00050-6).

Cundall PA, Strack ODL (1979) A discrete numerical model for granular assemblies. *Géotechnique* 29(1): 47-65. DOI: <http://doi.org/10.1680/geot.1979.29.1.47>.

Dong Y, Fu Z, Peng Y, Zheng Y, Yan H, Li X (2020) Precision fertilization method of field crops based on the Wavelet-BP neural network in China. *Journal of Cleaner Production* 246: 118735. DOI: <http://doi.org/10.1016/j.jclepro.2019.118735>.

Han Y, Jia F, Zeng Y, Jiang L, Zhang Y, Cao B (2016) Effects of rotation speed and outlet opening on particle flow in a vertical rice mill. *Powder Technology* 297: 153-164. DOI: <http://doi.org/10.1016/j.powtec.2016.04.022>.

Hanley KJ, O'Sullivan C, Oliveira JC, Cronin K, Byrne EP (2011) Application of Taguchi methods to DEM calibration of bonded agglomerates. *Powder Technology* 210(3): 230-240. DOI: <http://doi.org/https://doi.org/10.1016/j.powtec.2011.03.023>.

Hertz H (1881) On the contact of elastic solids. *Journal für die reine und angewandte Mathematik* (92): 156-171.

- Landry H, Laguë C, Roberge M (2006) Discrete element representation of manure products. *Computers and Electronics in Agriculture* 51(1-2): 17-34. DOI: <http://doi.org/10.1016/j.compag.2005.10.004>.
- Liu C, Wei D, Song J, Li Y, Du X, Zhang F (2018) Systematic study on boundary parameters of discrete element simulation of granular fertilizer. *Transactions of The Chinese Society for Agricultural Machinery* 49(09): 82-89.
- Mackay D (1992) Bayesian interpolation. *Neural Computation* 4(3): 415-447. DOI: <http://doi.org/10.1162/neco.1992.4.3.415>.
- Mindlin RD (1949) Compliance of elastic bodies in contact. *Journal of Applied Mechanics-Transactions of the Asme* 16: 259-268.
- Mindlin RD, Deresiewicz H (1953) Elastic spheres in contact under varying oblique forces. *ASME* 327-344.
- Müller D, Fimbinger E, Brand C (2021) Algorithm for the determination of the angle of repose in bulk material analysis. *Powder Technology* 383: 598-605. DOI: <http://doi.org/https://doi.org/10.1016/j.powtec.2021.01.010>.
- Qi J, Zhao W, Kan Z, Meng H, Li Y (2019) Parameter optimization of double-blade normal milk processing and mixing performance based on RSM and BP-GA. *Food Science & Nutrition* 7(11): 3501-3512. DOI: <http://doi.org/10.1002/fsn3.1198>.
- Rackl M, Hanley KJ (2017) A methodical calibration procedure for discrete element models. *Powder Technology* 307: 73-83. DOI: <http://doi.org/10.1016/j.powtec.2016.11.048>.
- Sakaguchi H, Ozaki E, Igarashi T (1993) Plugging of the flow of granular materials during the discharge from a silo. *International Journal of Modern Physics B* 7: 1949. DOI: <http://doi.org/10.1142/S0217979293002705>.
- Tan Y, Fottner J, Kessler S (2020) An efficient and reliable method for determining the angle of repose of biomass by using 3D scan. *Biomass and Bioenergy* 132: 105434. DOI: <https://doi.org/10.1016/j.biombioe.2019.105434>.
- Tan Y, Yu Y, Fottner J, Kessler S (2021) Automated measurement of the numerical angle of repose (aMAoR) of biomass particles in EDEM with a novel algorithm. *Powder Technology* 388: 462-473. DOI: <http://doi.org/10.1016/j.powtec.2021.04.062>.
- Tsuji Y, Tanaka T, Ishida T (1992) Lagrangian numerical simulation of plug flow of cohesionless particles in a horizontal pipe. *Powder Technology* 71(3): 239-250. DOI: [http://doi.org/https://doi.org/10.1016/0032-5910\(92\)88030-L](http://doi.org/https://doi.org/10.1016/0032-5910(92)88030-L)
- Wang Y, Zhang Y, Yang Y, Zhao H, Yang C, He Y, et al. (2020) Discrete element modelling of citrus fruit stalks and its verification. *Biosystems Engineering* 200: 400-414. DOI: <http://doi.org/10.1016/j.biosystemseng.2020.10.020>.
- Xia R, Li B, Wang X, Li T, Yang Z (2019) Measurement and calibration of the discrete element parameters of wet bulk coal. *Measurement* 142: 84-95. DOI: <http://doi.org/10.1016/j.measurement.2019.04.069>.
- Xiao Y, Han Y, Jia F, Liu H, Li G, Chen P, Meng X, Bai S (2021) Research on clogging mechanisms of bulk materials flowing through a bottleneck. *Powder Technology* 381: 381-391. DOI: <http://doi.org/10.1016/j.powtec.2020.11.067>.
- Yoon J (2007) Application of experimental design and optimization to PFC model calibration in uniaxial compression simulation. *International Journal of Rock Mechanics and Mining Sciences* 44(6): 871-889. DOI: <http://doi.org/10.1016/j.ijrmms.2007.01.004>.
- Zhang S, Tekeste MZ, Li Y, Gaul A, Zhu D, Liao J (2020) Scaled-up rice grain modelling for DEM calibration and the validation of hopper flow. *Biosystems Engineering* 194: 196-212. DOI: <http://doi.org/10.1016/j.biosystemseng.2020.03.018>.
- Zhou H, Hu Z, Chen J, Lv X, Xie N (2018) Calibration of DEM models for irregular particles based on experimental design method and bulk experiments. *Powder Technology* 332: 210-223. DOI: <http://doi.org/https://doi.org/10.1016/j.powtec.2018.03.064>.
- Zhu Q, Wu G, Chen L, Zhao C, Meng Z (2018) Influences of structure parameters of straight flute wheel on fertilizing performance of fertilizer apparatus. *Transactions of The Chinese Society of Agricultural Engineering* 34(18): 12-20.